Influences of Adsorption on TiO_2 Photocatalytic One-Electron Oxidation of Aromatic Sulfides Studied by Time-Resolved Diffuse Reflectance Spectroscopy

Takashi Tachikawa, Sachiko Tojo, Mamoru Fujitsuka, and Tetsuro Majima*

The Institute of Scientific and Industrial Research (SANKEN), Osaka University, Mihogaoka 8-1, Ibaraki, Osaka 567-0047, Japan

Received: October 6, 2003; In Final Form: March 4, 2004

TiO_2 photocatalytic one-electron oxidation of 4-methyl-*p*-tolylsulfide (MTS), 4-(methylthio)phenyl methanol (MTPM), 4-(methylthio)benzoic acid (MTBA), and 4-(methylthio)phenyl acetic acid (MTPA) adsorbed on the surface of TiO_2 powder slurried in acetonitrile (CH_3CN) has been investigated by time-resolved diffuse reflectance spectroscopy. As compared to MTS, high concentrations of the adsorbed MTPM, MTBA, and MTPA determined by UV absorption spectral measurements clearly indicate that −OH and −COOH groups play an important role in being adsorbed on the surface of TiO_2 particles. From Langmuir-type adsorption/desorption plots, the apparent equilibrium constants (K_{ad}) of 20, 60, 2.3×10^4, and 1.1×10^4 M^{-1} were determined for MTS, MTPM, MTBA, and MTPA, respectively. The difference in the K_{ad} values clearly indicates that −COOH and $-CH_2COOH$ groups are strongly adsorbed on the TiO_2 surface compared with $-CH_2OH$ and $-CH_3$ groups. The initial concentration of the radical cations generated from oxidation reactions with holes significantly depended on the concentration of substrate adsorbed on the TiO_2 surface. The relationship between the amount of adsorbates and the initial intensity was discussed in terms of Marcus theory. The decay kinetics for transient signals of the radical cations was also discussed.

1. Introduction

Titanium dioxide (TiO_2) has been extensively used as the photocatalyst for environmental cleanup because of its stability and nontoxicity.[1−6] It is well-known that electron−hole pairs are generated when TiO_2 is irradiated by UV photons with energy higher than the TiO_2 band gap energy (3.2 eV) and these charge carriers can migrate to the TiO_2 surface to initiate redox reactions with adsorbates. However, the mechanism of photooxidation on the TiO_2 surfaces is still under discussion.[7−15] It is proposed that the surface hydroxyl groups react with the holes to form the surface-bound OH radicals, which then oxidize the surface adsorbates. Support for this mechanism comes from the chemical identification of the hydroxylated oxidation intermediates, EPR detection of the surface OH radical in aqueous TiO_2 sols, the scavenging OH radicals, and the kinetic isotope effect.[8−10] Several researchers also reported that the surface-bound OH radicals are key species for the oxidation reaction because the diffusion of surface-bound OH radicals from the TiO_2 surface into the bulk solution is minimal.[9] Recently, Nosaka and co-workers investigated the adsorption and photodecomposition of ethanol in the presence of water adsorbed on the TiO_2 surface by solid-state ^1H NMR spectroscopy.[11] They concluded that decomposition reaction of ethanol molecules proceeded in physisorbed water layers.

Although a great deal of research has been conducted on the oxidation reactions between the OH radicals and variable substrates, little attention has been focused on the origin of the OH radicals and the subsequent reactivity of the transient species concerned with the oxidation processes. A proper understanding of the relationship between the adsorption dynamics and the oxidation kinetics of organic molecules on the TiO_2 surface must lead to novel developments of efficient photocatalytic systems specific to particular chemical species.

The time-resolved diffuse reflectance method is a powerful tool for investigations of photocatalysis in various conditions.[12−15] TiO_2 nanoparticles are only soluble over a limited pH range and generally soluble only in the solvent in which they are synthesized. In a nonaqueous medium, it is expected that the TiO_2 particle surfaces are main reaction fields of the direct oxidation. A time-resolved diffuse reflectance spectroscopy has been used to study the interfacial electron transfer between molecular adsorbate and wet TiO_2 powders. Fox and co-workers concluded that many oxidation reactions appear to occur by direct electron transfer from the photoexcited TiO_2 powder to a variety of substrates in CH_3CN.[12] However, only a few quantitative studies have been reported on the oxidation processes of organic molecules on the TiO_2 particle surface and the interactions between the substrate and the TiO_2 surface. Recently, we have studied the one-electron oxidation of several aromatic sulfides adsorbed on the surface of TiO_2 powder slurried in CH_3CN by nanosecond time-resolved diffuse reflectance spectroscopy and concluded that the −OH groups play an important role in the adsorption on the surface of TiO_2 and the efficiency of the one-electron oxidation of substrates.

In the present paper, we have investigated the influence of the adsorption on the oxidation kinetics of several aromatic compounds having −OH and −COOH groups (see insets in Figure 1) during the photoexcitation of the TiO_2 powder suspended in CH_3CN by steady-state and time-resolved diffuse reflectance absorption spectroscopies. The effects of the oxidation potentials of substrates on the one-electron oxidation of the substrates adsorbed on the TiO_2 surface and the relationship between the amount of adsorbates and the initial intensity are discussed in terms of Marcus theory. The decay kinetics for transient signals of the radical cations is also discussed.

* Address correspondence ot this author. E-mail: majima@sanken.osaka-u.ac.jp. Phone: +81-6-6879-8495. Fax: +81-6-6879-8499.

10.1021/jp037003t CCC: $27.50
Published on Web 04/15/2004

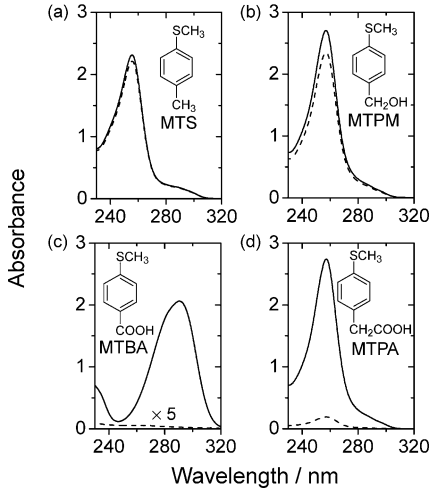

Figure 1. Steady-state UV absorption spectra of MTS (2 mM) (a), MTPM (2 mM) (b), MTBA (1 mM) (c), and MTPA (2 mM) (d) in CH_3CN at room temperature. Solid lines indicate the spectra observed for substrates in bulk CH_3CN. Broken lines indicate those observed for substrates after reaching the adsorption equilibrium in CH_3CN. Inset: structures of MTS, MTPM, MTBA, and MTPA.

2. Experimental Section

2.1. Materials. TiO_2 powder (P25, Japan Aerosil) was a mixture of rutile (20%) and anatase (80%) with a BET surface area of 50 $m^2\ g^{-1}$ and an average primary particle size of 21 nm. 4-Methyl-*p*-tolyl sulfide (MTS) (Tokyo Kasei) was used without further purification. 4-(Methylthio)phenylmethanol (MTPM) (Aldrich) was purified by vacuum sublimation before use. 4-(Methylthio)benzoic acid (MTBA) and 4-(methylthio)-phenylacetic acid (MTPA) were recrystallized from ethanol. The molecular structures of MTS, MTPM, MTBA, and MTPA are shown in Figure 1. Fresh CH_3CN (Nakarai Tesque, spectral grade) was used as the solvent without further purification.

2.2. Steady-State UV−Vis Absorption and Diffuse Reflectance Spectral Measurements. Steady-state UV−vis absorption and diffuse reflectance spectra were measured by UV−vis−near-IR spectrophotometers (Shimadzu, UV-3100, and Jasco, V-570, respectively) at room temperature. The sample solutions containing TiO_2 powder (20 g dm^{-3}) were sonicated for 10 min and TiO_2 particles in solution were then completely removed by the centrifugation (10 000 rpm, 10 min), using a high-speed microcentrifuge (Hitachi, himac CF16RX) at 22 °C for UV absorption measurements. All procedures for the sample preparation were performed with shielding from the UV light.

2.3. Transient Diffuse Reflectance Measurements. Time-resolved diffuse reflectance measurements were performed by using the third harmonic generation (355 nm, 5 ns full width at half-maximum) from a Q-switched Nd^{3+}:YAG laser (Continuum, Surelite II-10) and 430-nm flash from an OPO laser (Continuum, Surelite) pumped by a Q-switched Nd^{3+}:YAG laser (Continuum, Surelite II-10) for the excitation operated with temporal control by a delay generator (Stanford Research Systems, DG535). In the experiments, the spot irradiated on the sample cell with a thickness of 2 mm was approximately 1 cm^2. The reflected analyzing light from a pulsed 450-W Xe-arc lamp (Osram, XBO-450) was collected by a focusing lens and directed through a grating monochromator (Nikon, G250) to a photomultiplier tube (Hamamatsu Photonics, R928). The transient signals were recorded with a digitizer (Tektronix, TDS 580D). The reported signals are averages of 64−128 events.

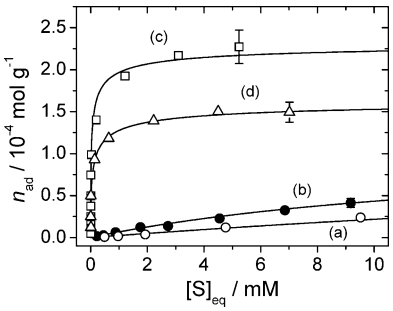

Figure 2. Langmuir adsorption plots for MTS (a), MTPM (b), MTBA (c), and MTPA (d) in CH_3CN (5×10^{-3} dm^3) containing TiO_2 powder (100 mg). The solid lines are the best fits obtained by the calculations based on eqs 1 and 2.

3. Results

3.1. Adsorption Isotherms. The concentrations of the adsorbates in CH_3CN containing TiO_2 powder (20 g dm^{-3}) after reaching adsorption equilibrium ($[S]_{eq}$) were determined from steady-state UV absorption measurements. Figure 1 depictes the UV absorption spectra observed for MTS (a), MTPM (b), MTBA (c), and MTPA (d) in CH_3CN at room temperature. For example, Figure 1b shows the absorption spectra of 2 mM (M ≡ mol dm^{-3}) MTPM in bulk CH_3CN (solid line) and MTPM in CH_3CN after reaching adsorption equilibrium with the surface of TiO_2 particles (broken line). The TiO_2 particles in solution, here, were completely removed by the centrifugation (10 000 rpm, 10 min). The absorbance of the absorption spectrum of MTPM in CH_3CN after reaching the adsorption equilibrium indicated the reduction of 9%, compared to that of MTPM in CH_3CN in the absence of TiO_2 powder. This result clearly suggests the adsorption of MTPM molecules on the surface of TiO_2 particles in solution. The remarkable substrate adsorptions were observed for MTBA and MTPA as shown in Figure 2c,d. On the other hand, MTS hardly can be adsorbed on the TiO_2 surface.

Figure 2 shows the adsorption isotherm of MTS (a), MTPM (b), MTBA (c), and MTPA (d) on the TiO_2 surface in CH_3CN at room temperature, where the amount of equilibrium adsorption, n_{ad}, in the number of adsorbed substrates per gram of TiO_2 was plotted as a function of the equilibrium substrate concentration in the bulk solution, $[S]_{eq}$. The n_{ad} values were calculated from the difference in the absorbance with and without TiO_2 powder in solutions. According to the Langmuir adsorption models for a single bond structure and a bidentate binuclear bond structure on the solid−liquid interface,[16−19] n_{ad} can be expressed by the following equations,

$$n_{ad} = \frac{K_{ad}[S]_{eq}}{1 + K_{ad}[S]_{eq}} n_s \quad (1)$$

$$n_{ad} = \frac{K_{ad}^{1/2}[S]_{eq}^{1/2}}{1 + K_{ad}^{1/2}[S]_{eq}^{1/2}} n_s \quad (2)$$

respectively, where n_s is the total number of adsorption sites and K_{ad} is the equilibrium constant of adsorption. The $[S]_{eq}$ dependences of n_{ad} for MTS and MTPM were quite reproducible from the Langmuir adsorption model for a single bond structure (eq 1), while those for MTBA and MTPA were reproduced from the Langmuir adsorption model for a bidentate binuclear bond structure (eq 2), although this model does not provide a perfect fit at $[MTBA]_{eq} > 1$ mM. Here, we assumed the bridge and

TABLE 1: Equilibrium Constants of Adsorption (K_{ad}) and the Total Amount of Adsorption Sites (n_s) Obtained from Langmuir Plots for MTS, MTPM, MTBA, and MTPA As Shown in Figure 2

substrate	K_{ad}/M^{-1}	$n_s/10^{-4}$ mol g^{-1}
MTS	20 ± 5	1.2
MTPM	60 ± 10	1.2
MTBA	$(2.3 \pm 0.4) \times 10^4$	2.3
MTPA	$(1.1 \pm 0.2) \times 10^4$	1.4

double hydrogen bonding type adsorption between the $-$COOH group and the TiO_2 surface.[20] The n_s and K_{ad} values obtained for MTS, MTPM, MTBA, and MTPA were summarized in Table 1. The observed n_s values are larger than the 5.4×10^{-5} mol g^{-1} reported for benzyl alcohol adsorbed on the TiO_2 powder (Degussa, P25) in CH_3CN.[21] The K_{ad} values of 20 ± 5, 60 ± 10, $2.3 \pm 0.4 \times 10^4$, and $1.1 \pm 0.2 \times 10^4$ M^{-1} were determined for MTS, MTPM, MTBA, and MTPA, respectively. The difference in K_{ad} values clearly indicates that $-$COOH and $-CH_2COOH$ groups are strongly adsorbed on the TiO_2 surface, compared with $-CH_2OH$ and $-CH_3$ groups.

3.2. Time-Resolved Diffuse Reflectance Absorption. Transient diffuse reflectance absorption spectra were observed during the laser photolysis of TiO_2 with 355-nm light (1.5 mJ $pulse^{-1}$) in the absence and presence of MTPM, MTBA, and MTPA in CH_3CN at room temperature.

Figure 3a shows the transient diffuse reflectance absorption spectra obtained during the laser photolysis of TiO_2 (20 g dm^{-3}) with 355-nm light in the absence of substrates in CH_3CN. A transient absorption band with a maximum around 560 nm appeared immediately after the laser flash and was assigned to the trapped electron as reported elsewhere.[22−24] The broad transient absorption band below 460 nm was also observed. This band is assigned to the trapped holes or surface-bound hydroxyl radical.[25−27] These transient species show the long lifetime with additions of O_2 and methanol as electron and hole acceptors, respectively. Therefore, we assumed these stable species are the deep trapped species and cannot react with the substrates adsorbed on the TiO_2 surface in the present time region. The absorption values attributed to substrates (%absorption) were obtained by subtracting the absorption value observed in the absence of substrates from that observed in the presence of substrates. Here, percent absorption (% abs) is given by eq 3,

$$\%\ \text{abs} = \frac{R_0 - R}{R_0} \times 100 \qquad (3)$$

where R and R_0 represent intensities of the diffuse reflected monitor light with and without excitation, respectively.[14,15,28]

Figure 3b shows the transient diffuse reflectance absorption spectra obtained during the laser photolysis of TiO_2 with 355-nm light in the presence of MTPM (10 mM) in CH_3CN. The transient absorption band at 500−700 nm appeared immediately after the laser flash and was assigned to the MTPM radical cation ($MTPM^{\bullet+}$), although the spectral shape was about 1.5 times broader than that obtained during the pulse radiolysis of N_2O-saturated aqueous solution in the presence of MTPM.[29] This broad spectrum clearly indicates the interaction between $MTPM^{\bullet+}$ and TiO_2 particle surface. Panels c and d in Figure 3 show the transient diffuse reflectance absorption spectra obtained during the laser photolysis of TiO_2 with 355-nm light in the presence of MTBA (1 mM) and MTPA (2 mM) in CH_3CN, respectively. The broad transient absorption band at 450−650 nm was observed immediately after the laser flash and assigned to the radical cation of MTBA ($MTBA^{\bullet+}$) as shown in Figure 3c.[30] Similar transient spectra were observed for MTPA as shown in Figure 3d. Therefore, we assigned the transient absorption band with a maximum peak at 550 nm shown in Figure 3d to that of $MTPA^{\bullet+}$.[31] In the case of MTS, we could not observe the transient spectra because of the weak signal intensity.[15]

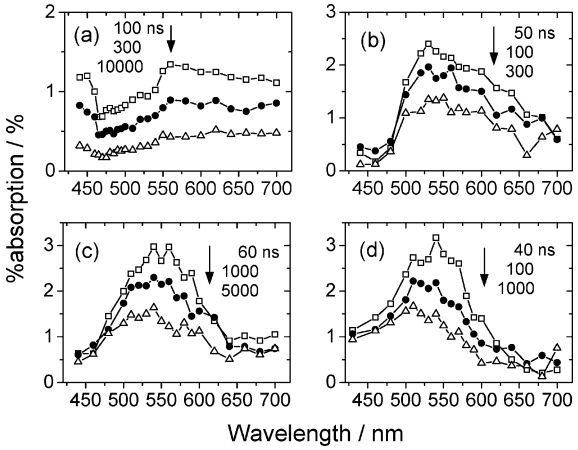

Figure 3. Transient diffuse reflectance absorption spectra obtained at 100 (solid squares), 300 (solid circles), and 10000 ns (solid triangles) after a laser flash during the 355-nm laser photolysis of TiO_2 powder in the absence of substrate in CH_3CN (a). Transient diffuse reflectance absorption spectra obtained at 50 (solid squares), 100 (solid circles), and 300 ns (solid triangles) after a laser flash during the 355-nm laser photolysis of TiO_2 powder in the presence of MTPM (10 mM) in CH_3CN (b). Transient diffuse reflectance absorption spectra obtained at 60 (solid squares), 1000 (solid circles), and 5000 ns (solid triangles) after a laser flash during the 355-nm laser photolysis of TiO_2 powder in the presence of MTBA (1 mM) in CH_3CN (c). Transient diffuse reflectance absorption spectra obtained at 40 (solid squares), 100 (solid circles), and 1000 ns (solid triangles) after a laser flash during the 355-nm laser photolysis of TiO_2 powder in the presence of MTPA (2 mM) in CH_3CN (d).

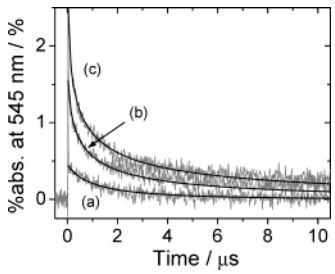

Figure 4. The percent absorption at 545 nm vs time after a laser flash during the 355-nm laser flash photolysis of TiO_2 powder in the presence of MTPM (1 (a), 5 (b), 10 mM (c)). Solid lines indicate simulation results fitted by the Albery model (eq 4).

Figure 4 shows the time traces observed at the 545-nm absorption obtained by the laser photolysis of TiO_2 with 355-nm light in the presence of MTPM (1 (a), 5 (b), and 10 mM (c)). The decay kinetics of the absorption was fitted by the Albery model,[12,32] as given by eq 4, where % $abs^{t=0}$ denotes

$$\frac{\%\ \text{abs}}{\%\ \text{abs}^{t=0}} = \int_{-\infty}^{+\infty} \frac{\exp(-x^2)\ \exp[-k_{\bar{d}} t\ \exp(\gamma x)]\ \mathrm{d}x}{\exp(-x^2)\ \mathrm{d}x} \qquad (4)$$

the percent absorbance value at $t = 0$, γ is the parameter describing the width of the distribution of the average deactivation rate constant ($k_{\bar{d}}$), and x is the distribution variable, being allowed to take values between plus and minus infinity. In the limit of $\gamma = 0$, this expression reduces to an ordinary first-order rate law. Since the integral has no analytical solution, this

TABLE 2: Initial Concentration ([S]), the Amount of Adsorbate (n_{ad}), Percent Absorption at $t = 0$ (% abs$^{t=0}$), and Kinetic Parameters As Given by Eq 4

substrate	[S]/mM	$n_{ad}/10^{-4}$ mol g^{-1}	% abs$^{t=0}$/%	$k_d/10^6$ s^{-1}	γ
MTS	0.5	0.01			
	1	0.02			
	2	0.04	0.17	0.22	1.0
	5	0.12	0.34	0.24	1.0
	10	0.24	0.48	0.20	0.8
MTPM	0.5	0.03	0.25	0.6	1.0
	1	0.06	0.5	0.8	1.2
	2	0.12	1.0	1.0	2.0
	5	0.23	1.6	1.3	2.3
	7.5	0.33	2.0	1.5	2.3
	10	0.41	2.6	1.7	2.7
MTBA	0.1	0.04	0.93	0.45	1.6
	0.25	0.12	1.6	0.47	2.0
	0.4	0.20	2.7	0.45	3.2
	0.5	0.25	3.2	0.42	3.7
	0.75	0.37	3.6	0.45	3.8
	1	0.50	4.2	0.42	3.9
	1.5	0.75	4.0	0.40	4.0
	2	0.99	2.8	0.55	3.8
	3	1.40	2.2	0.75	2.5
	5	1.92	1.7	0.85	2.2
	7.5	2.17	1.4	1.2	1.2
	10	2.27	0.66		
MTPA	0.25	0.12	0.44	0.22	1.5
	0.5	0.25	1.1	0.28	3.0
	1	0.50	1.5	0.32	3.3
	2	0.93	3.1	0.34	3.6
	3	1.18	4.1	0.36	3.8
	5	1.39	4.0	0.37	3.6
	7.5	1.50	4.3	0.37	3.7
	10	1.49	3.9	0.25	3.7

TABLE 3: Oxidation Potentials (E_{ox}/V vs NHE) of Several Oxidizing Species and Substrates

h_{VB}^{+} [a]	$OH_{surf}^{\bullet}$ [b]	$OH_{free}^{\bullet}$ [c]	MTS[d]	MTPM[d]	MTBA[d]	MTPA[d]
2.66	1.5	1.9	1.57	1.59	1.86	1.67

[a] Calculated from $E_{CB} = -0.13 - 0.059$ pH, ref 34. [b] From ref 26. [c] From ref 35. [d] From ref 36.

model has been successfully applied to heterogeneous powders and powder suspensions.[12,32,33] The determined parameters were summarized in Table 2. The decay kinetics of the radical cation is discussed in Section 4.3.

Figure 5 shows the substrate concentration ([S]) dependence of % abs$^{t=0}$ for MTS, MTPM, MTBA, and MTPA. The % abs$^{t=0}$ increased with increasing [S] in the present concentration except for MTBA, suggesting that substrate radical cation ($S^{\bullet+}$) is generated by the bimolecular reaction with the photogenerated oxidizing species on the TiO_2 surface. The % abs$^{t=0}$ values obtained at [S] = 10 mM show the relationship of MTPA > MTPM ≫ MTS, clearly suggesting that the concentrations of $S^{\bullet+}$ depend on the amount of substrates adsorbed on the TiO_2 surface in CH_3CN. Specifically, small % abs$^{t=0}$ values were obtained for $MTS^{\bullet+}$ despite a relatively large molar extinction coefficient and an almost identical oxidation potential, compared with MTPM as summarized in Table 3. These results clearly indicate the −OH and −COOH groups play an important role in the TiO_2 photocatalytic reaction on the surface of TiO_2 particles in CH_3CN.

In the case of MTBA, the increases in signal intensity observed at the low MTBA concentrations (<1.0 mM) are much larger than those of other substrates. The color of the sample solutions also changed from white to yellow at ~3 mM. Figure 6 shows the diffuse reflectance spectra observed for TiO_2 slurries in the presence of MTBA (1 (a), 3 (b), 5 (c), and 10 mM (d)).

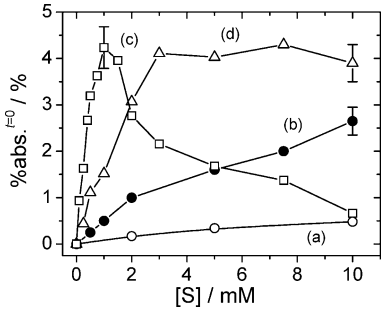

Figure 5. Substrate concentration dependence of the % abs$^{t=0}$ values obtained for MTS (a), MTPM (b), MTBA (c), and MTPA (d). Solid lines are guides for the eyes.

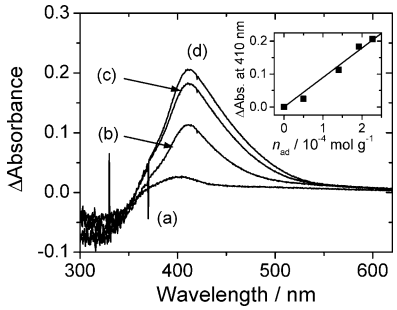

Figure 6. Steady-state diffuse reflectance difference spectra observed for the TiO_2 slurry containing with MTBA of 1 (a), 3 (b), 5 (c), and 10 mM (d) at room temperature (Δabsorbance = absorbance (TiO_2 + MTBA) − absorbance (TiO_2)). Inset: The relationship between the Δabsorbance and the amount of absorbed substrate (n_{ad}).

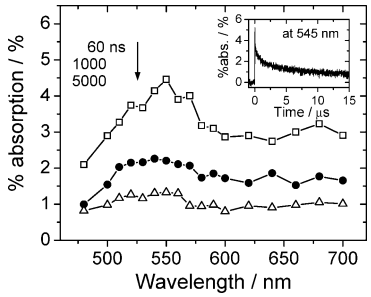

Figure 7. Transient diffuse reflectance absorption spectra obtained at 60 (solid squares), 1000 (solid circles), and 5000 ns (solid triangles) after a laser flash during the 430-nm laser photolysis of TiO_2 powder in the presence of MTBA (10 mM) in CH_3CN. Inset: The % absorption at 545 nm vs time after a laser flash during the 430-nm laser flash photolysis of TiO_2 powder in the presence of MTPM (10 mM).

The Δabsorbance values, defined as the difference in absorbances of spectra observed for samples in the presence and the absence of MTBA, show a linear relationship with the n_{ad} values, clearly indicating the formation of the charge transfer (CT) complex between the MTBA and TiO_2. The observed CT band is very similar to that observed for catechol and the TiO_2 nanoparticle.[17,37]

We also observed the transient diffuse reflectance spectra and strong transient signals depended on the MTBA concentration (>2 mM) during the 430-nm laser photolysis of the CT band in CH_3CN at room temperature. Figure 7 shows the transient diffuse reflectance absorption spectra obtained at 60, 1000, and 5000 ns after a laser flash during the 430-nm laser photolysis (1.5 mJ pulse^{-1}) of TiO_2 powder in the presence of MTBA (10 mM) in CH_3CN. A broad transient absorption spectrum ranging from 600 to 700 nm was observed immediately after a laser flash. It seems that the decreases in signal intensities observed at the high MTBA concentration (>2 mM) are attributable to

the bimolecular reaction between the $MTBA^{\bullet+}$ and adsorbates as discussed in Section 4.3.

4. Discussion

4.1. Effective Oxidation Species on the TiO_2 Surface. It is well-established that, under the band gap excitation, TiO_2 particles generate electron−hole pairs (eq 5).

$$TiO_2 \xrightarrow{h\nu} h_{VB}^{+} + e_{CB}^{-} \tag{5}$$

After their generation within the short light pulse, both electron and hole are extremely rapidly trapped in surface states of the semiconductor particle within subpicoseconds or a few picoseconds after excitation (eqs 6 and 7).

$$h_{VB}^{+} \rightarrow h_{tr}^{+} \tag{6}$$

$$e_{CB}^{-} \rightarrow e_{tr}^{-} \tag{7}$$

As already mentioned in the Introduction, these photogenerated carriers migrate to the particle surface and participate in redox processes at the surface. The trapped electron exhibits the strong transient absorption around 650 nm, while the trapped hole absorbs at shorter wavelengths, around 430 nm. As a result, a very broad, featureless transient absorption spectrum ranging from 400 to 800 nm is consequently observed immediately after a laser flash. The fast recombination kinetics of the trapped charge carriers have been studied in detail by several groups.[22−25] The most trapped charge carriers recombine quickly, i.e., within less than 30 ps (eq 8),[38] while a minority in deeper traps survive

$$e_{tr}^{-} + h_{VB}^{+} (h_{tr}^{+}) \rightarrow \text{heat}, \tag{8}$$

and will be available for reactions with substrates such as O_2. Therefore, we subtracted the transient signal attributed to the nonreactive trapped electron and hole from the observed transient signals at each experimental condition as mentioned above.

According to previous research, the trapped charges can react with various dissolved and adsorbed components. The trapped positive hole, like the surface-bound OH radical, typically oxidizes an organic molecule and thus induces its further oxidative degradation, while the trapped electron, like the surface-bound Ti^{3+}, typically reduces dioxygen to the superoxide radical anion. The surface-trapped hole is chemically equivalent to a surface-bound OH radical, which can initiate the primary oxidation reaction of substrates adsorbed on the TiO_2 surface before diffusing into the bulk solution. In the present systems, the transient absorption signals attributed to the radical cation of substrates ($S^{\bullet+}$) were observed immediately after an excitation laser pulse, clearly suggesting that the oxidation of substrates occurred by the trapped positive hole (eq 9) or surface-bound OH radicals (eqs 10 and 11) at the surface on TiO_2 in CH_3CN solution within a laser pulse duration.

$$h_{VB}^{+} (h_{tr}^{+}) + S \rightarrow S^{\bullet+} \tag{9}$$

$$h_{VB}^{+} (h_{tr}^{+}) + OH_{surf}^{-} \rightarrow OH_{surf}^{\bullet} \tag{10}$$

$$OH_{surf}^{\bullet} + S \rightarrow S^{\bullet} + + OH^{-} \tag{11}$$

We observed the fast formation of $S^{\bullet+}$ within a laser pulse duration by the laser flash photolysis of the TiO_2 powder in CH_3CN with 355-nm light in the presence of substrates. This fast formation of $S^{\bullet+}$ was also observed by the laser flash photolysis of the colloidal TiO_2 aqueous sample with 355-nm light in the presence of MTPM (≥1 mM).

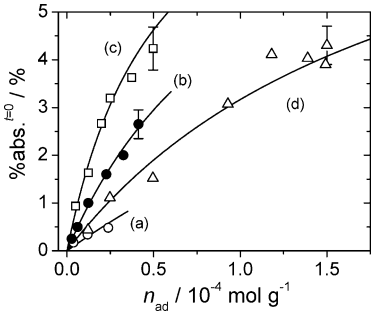

Figure 8. The relationship between the % abs$^{t=0}$ and the amount of absorbed substrate (n_{ad}) obtained for MTS (a), MTPM (b), MTBA (c), and MTPA (d). The lines are guides for the eyes.

According to the Marcus theory, the free energy change for a charge separation (ΔG_{ct}) is simply given by eq 12, where E_S

$$\Delta G_{ct} = E_S - E_{ox} \tag{12}$$

and E_{ox} are the oxidation potentials of S and oxidizing species, respectively. The oxidation potentials of S and several oxidizing species were summarized in Table 3. It is clear that MTBA can hardly react with $OH_{free}^{\bullet}$ and $OH_{surf}^{\bullet}$, because the ΔG_{ct} values are close to zero or positive, respectively. Therefore, we assume that h_{VB}^{+} is a main oxidizing species in the present systems. As indicated in Table 3, h_{VB}^{+} has the E_{ox} of 2.66 V vs NHE, which is a flat band potential of the valence band.[34] In this case, it is possible that h_{VB}^{+} can oxidize MTBA.

4.2. Effects of Adsorption on the Oxidation Reaction of Substrates. In the case of the present experiments, it is not possible to use the Kubelka−Monk formalism, so we do not know our absolute concentration of $S^{\bullet+}$. However, one can extract the relative change of the $S^{\bullet+}$ concentration from the initial signal intensity due to the fact that the signal intensity is proportional to transient concentrations.[12,14,28]

Figure 8 shows the relationship between the concentration of substrates adsorbed on the TiO_2 surface (n_{ad}) and % abs$^{t=0}$. The % abs$^{t=0}$ values were found to be approximately proportional to the n_{ad} values in the present concentrations. As an oxidation reaction rate (k_{ox}) of the substrate by h_{VB}^{+} competes with the fast recombination reaction rate (k_r), the observed quantum yield of $S^{\bullet+}$ generated by the oxidation reaction (ϕ_{ox})[39] is tentatively given by eq 13.

$$\phi_{ox} = \frac{k_{ox} n_{ad}}{k_r + k_{ox} n_{ad}}. \tag{13}$$

As $k_r \geq k_{ox} n_{ad}$, the ϕ_{ox} values are approximately proportional to the n_{ad} values.

According to the treatments for a heterogeneous charge transfer,[40] the k_{ox} value is describe by eq 14, where k_{ct} is the

$$\frac{1}{k_{ox}^{obs}} = \left(\frac{1}{4\pi R^2}\right)\left(\frac{1}{k_{ct}} + \frac{R}{D}\right) \tag{14}$$

charge-transfer rate constant (units cm s^{-1}), R is the sum of the radii of the TiO_2 particle and the hole acceptor, and D is the sum of their respective diffusion coefficients. Since the influence of diffusion can be eliminated by adsorption at the TiO_2 surface, k_{ct} is simply described by eq 15, where δ is the reaction layer

$$k_{ct} = \delta/\tau_{ct} \tag{15}$$

thickness and τ_{ct} is the average time required for the charge carrier to tunnel across the interface and given by eq 16, where

$$\tau_{ct}^{-1} = \frac{2\pi}{\hbar}|V(d)|^2 \times (FC) = \nu_0 \exp(-\beta(d - d_0)) \exp(-(\Delta G_{ct} + \lambda)^2/4\lambda kT) \quad (16)$$

λ is the reorganization energy ($\lambda = \lambda_v + \lambda_s$, λ_v, and λ_s are the intramolecule vibrational and solvent reorganization energies, respectively), and λ_s for the charge transfer on the semiconductor−liquid interface[41,42] is given by eq 17, where ϵ_0 is

$$\lambda_s = \frac{1}{2}\frac{(\Delta e)^2}{4\pi\epsilon_0}\left[\frac{1}{a}\left(\frac{1}{n^2} - \frac{1}{\epsilon}\right) - \frac{1}{2r}\left(\frac{n_{TiO}^2 2 - n^2}{n_{TiO}^2 2 + n^2}\,\frac{1}{n^2} - \frac{\epsilon_{TiO_2} - \epsilon}{\epsilon_{TiO_2} + \epsilon}\,\frac{1}{\epsilon}\right)\right] \quad (17)$$

the vacuum permittivity, ϵ is the static dielectric constant of the solvent ($\epsilon = 35.94$ for CH_3CN at 25 °C), n is the refractive index of the solvent ($n = 1.344$ ($n^2 = 1.806$) for CH_3CN at 25 °C), n_{TiO_2} and ϵ_{TiO_2} are n and ϵ for anatase TiO_2 ($n_{TiO_2} = 2.5$ ($n_{TiO_2}^2 = 6.3$) and $\epsilon_{TiO_2} = 86$).[43] We obtained the value of $\lambda_s = 0.7$ eV from eq 17. Using the decay factor β of 12 nm^{-1}, the λ_v of 0.3 eV,[44] the rate constant of the optimally exothermic electron transfer between species in contact distance ν_0 of 10^{13} s^{-1}, ($d - d_0$) of 0.5 nm,[40a] the mean electron-transfer distance r of 0.4 nm, and the molecular radius a of 0.40 nm,[45] we obtained the τ_{ct}^{-1} values of 2.5×10^{10}, 1.3×10^{10}, and 2.4×10^{10} s^{-1} for MTPM, MTBA, and MTPA, respectively, from eq 16. Since the δ is about $1/\beta \approx 0.083$ nm, the k_{ct} values of 2.0×10^{-2}, 1.0×10^{-2}, and 2.0×10^{-2} cm s^{-1} were estimated for MTPM, MTBA, and MTPA, respectively, from eq 15.

As mentioned above, the most free and trapped charge carriers recombine quickly, i.e., within less than 30 ps (eq 8). The average transit time (τ_{av}) for the hole from the interior to the surface of the particle can be calculated by eq 18, where r is

$$\tau_{av} = r^2/\pi^2 D_h \quad (18)$$

the radius of the particles and D_h is the diffusion coefficient of the hole at room temperature ($D_h = 4 \times 10^{-5}$ m^2 s^{-1}).[46] We obtained the secondary particle size of P25 TiO_2 powder of ~2 μm in CH_3CN from the dynamic light-scattering measurements. Here, we assumed that only a part of the surface of the aggregated TiO_2 powder is illuminated by a laser light and then estimated the penetration depth (r_0) of light into TiO_2 (~30 nm) from eq 19, where λ_{ex} is the wavelength of irradiation light (λ_{ex} = 355 nm) and k is the imaginary refractive index ($k = 1.0$).[47]

$$r_0 = \lambda_{ex}/4\pi k \quad (19)$$

We obtained τ_{av} of about 2 ps from eqs 18 and 19. This transit time of the hole is shorter than τ_{ct} values estimated from eq 16 for MTPM, MTBA, and MTPA, suggesting that τ_{ct}^{-1} values would control the overall reaction rates.

As shown in Figure 8, the efficiency of one-electron oxidation, that is % $abs^{t=0}/n_{ad}$, decreased in the order of MTBA > MTPM > MTPA > MTS. For example, at $n_{ad} \approx 0.12 \times 10^{-4}$ mol g^{-1}, the % $abs^{t=0}$ value obtained for MTPM is about 3 times larger than that for MTS despite almost the same oxidation potentials. These results suggest that interaction between MTPM and the TiO_2 surface, such as a hydrogen bonding, plays an important role in the oxidation kinetics. It seems that such interaction induces the large electronic coupling between the electron acceptor and the donor, resulting in an acceleration of the electron-transfer reaction rate. This tendency is suggested by the comparison between MTPM (b) and MTBA (d). The high efficiency of oxidation obtained for MTBA, compared to MTPM which has a higher E_{ox} and lower maximum molar extinction coefficient value of $S^{\bullet+}$ (5500 and 2300 M^{-1} cm^{-1} for $MTPM^{\bullet+}$ and $MTBA^{\bullet+}$, respectively),[29,30] is attributable to the formation of the CT complex between substrate and TiO_2. The relatively large % $abs^{t=0}$ values obtained for $MTBA^{\bullet+}$ generated by the laser photolysis of the CT band (430-nm excitation), compared with that by the laser photolysis of TiO_2 powder (355-nm excitation), are due to the direct oxidation processes, in other words, the oxidation reaction of S in the case of CT band excitation does not compete with the charge recombination reaction between the photogenerated hole and electron.

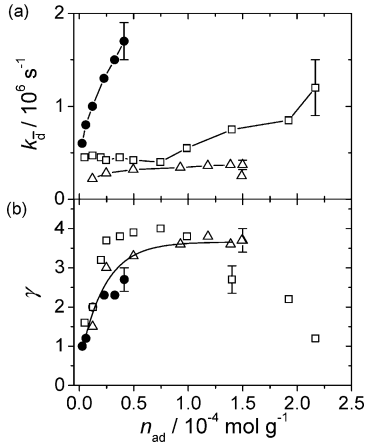

Figure 9. The n_{ad} dependences of the decay rate ($k_{\bar{d}}$) (a) and inhomogeneous parameter (γ) (b) observed for MTPM (solid circles), MTBA (open squares), and MTPA (open triangles). The lines are guides for the eyes.

4.3. Decay of Transient Signals. As shown in Figure 9, the $k_{\bar{d}}$ and γ values increased with increasing substrate concentration. This tendency is very similar to that obtained for another oxidation reaction system.

It is worth clarifying the sequential reactions caused by $S^{\bullet+}$, because the efficiency of the photocatalytic reaction would be significantly dependent on the interfacial back electron-transfer rate that competes with many others. The observation of distributed first-order kinetics may be explained in two ways. The first involves the back electron transfer.[48,49] The back electron-transfer reaction between the trapped electrons and $S^{\bullet+}$ was influenced by numerous factors, for example, a relaxation time from shallow to deep trap states, the oxidation potential of substrates, and the distance between the electron acceptor and the donor. Back electron transfer is thermodynamically favorable since the oxidation potential of $S^{\bullet+}$ is in the range of 1.59−1.86 V vs NHE, while that of molecular oxygen is −0.13 V vs NHE. We expect that the large excess of adsorbed molecular oxygen relative to $S^{\bullet+}$ would cause electron transfer to oxygen to be kinetically favorable. However, we observed almost the same signal traces for the oxygen and argon gas saturated samples.

In the present system, the signal intensity of $S^{\bullet+}$ increased with increasing the laser intensity, while $k_{\bar{d}}$ remained relatively constant, suggesting that disappearance of $S^{\bullet+}$ on the surface of the TiO_2 powder suspended in CH_3CN followed the first-order kinetics with a distribution of reaction rate constants. These results are quite consistent with that obtained for $(SCN)_2^{\bullet-}$ on the surface of TiO_2 powder suspended in water reported by Fox et al.[12a] These results clearly suggest the deactivation of $S^{\bullet+}$ is mainly attributable to the bimolecular reaction with adsorbates,

although the reaction schemes are unclear. It seems that remarkable γ values observed at the high substrate concentrations are attributable to the differences in the reactivity of S adsorbed on the heterogeneous surface of TiO_2 powder.

In the case of MTBA, as shown in Figure 5, the transient signal intensities decreased with increasing substrate concentration ([MTBA] > 2 mM). This tendency was observed for other systems at high concentrations ([S] > 10 mM). Recently, Sawaki et al. investigated the one-electron oxidation processes of aromatic sulfides in CH_3CN by the laser flash photolysis method and concluded that the dimer radical cations absorbing at around 460−500 nm are assigned to the σ-type complex of the sulfur−sulfur three-electron bond and that the radical cations absorbing at around 800 nm are of the π-type complex associated with two phenylthio groups.[50] They also suggested that the formation of dimer radical cation is very sensitive to the substrate concentration and the steric and electronic influence of substituents. As shown in Figure 7, the absorption band observed for the MTBA system is similar to those for the dimer radical cations of thioanisoles, such as *p*-chloro- and *p*-methylthioanisole.[50] Therefore, we conclude that the formation processes of the σ-type and π-type dimer radical cation are involved in the reaction dynamics of $MTBA^{\bullet+}$ on the TiO_2 surface at high MTBA concentrations. However, we could hardly observe the absorption band due to the dimer radical cations of other substrates at the present concentrations.

5. Conclusions

TiO_2 photocatalytic one-electron oxidation reactions of MTS, MTPM, MTBA, and MTPA adsorbed on the surface of TiO_2 powder slurried in CH_3CN were observed by time-resolved diffuse reflectance spectroscopy. As compared to MTS, high concentrations of the adsorbed MTPM and MTPA determined by UV absorption spectral measurements clearly indicate that −OH and −COOH groups play an important role in being adsorbed on the surface of TiO_2 particles. From Langmuir-type adsorption plots, the apparent equilibrium constants (K_{ad}) of 20, 60, 2.3×10^4, and 1.1×10^4 M^{-1} were determined for MTS, MTPM, MTBA, and MTPA, respectively. The initial concentration of the radical cations generated from the one-electron oxidation reactions with the photogenerated holes such as h_{VB}^+ significantly depended on [S]. The efficiency of one-electron oxidation decreased in the order of MTBA > MTPM > MTPA > MTS. These results suggest that the chemical bonding between substrates and the TiO_2 surface plays an important role in the oxidation kinetics as well as adsorption on the surface of TiO_2 particles. It seems that the CT interaction induces the large electronic coupling between the electron acceptor and the donor, resulting in an acceleration of the electron-transfer reaction rate and the high efficiency of the oxidation reaction.

Acknowledgment. This work has been partly supported by a Grant-in-Aid for Scientific Research on Priority Area (417), 21st Century COE Research, and others from the Ministry of Education, Culture, Sports, Science and Technology (MEXT) of the Japanese Government.

References and Notes

(1) (a) Fujishima, A.; Rao, T. N.; Tryk, D. A. *J. Photochem. Photobiol. C*: *Photochem. Rev.* **2000**, *1*, 1. (b) Fujishima, A.; Hashimoto, K.; Watanabe, T. *TiO_2 Photocatalysis*: *Fundamentals and Applications*; BKC, Inc.: Tokyo, Japan, 1999.

(2) (a) Mills, A.; Davies, R. H.; Worsley, D. *Chem. Soc. Rev.* **1993**, 417. (b) Mills, A.; Hunte, S. L. *J. Photochem. Photobiol. A* **1997**, *108*, 1.

(3) Ollis, D. F.; Al-Ekabi, H., Eds. *In Photocatalytic Purification and Treatment of Water and Air*; Elsevier: London, UK, 1993.

(4) Hoffmann, M. R.; Martin, S. T.; Choi, W.; Bahnemannt, D. W. *Chem. Rev.* **1995**, *95*, 69.

(5) Fox, M. A.; Dulay, M. T. *Chem. Rev.* **1993**, *93*, 341.

(6) (a) Kamat, P. V. *Chem. Rev.* **1993**, *93*, 267. (b) Kamat, P. V. *J. Phys. Chem. B* **2002**, *106*, 7729.

(7) (a) Nakamura, R.; Imanishi, A.; Murakoshi, K.; Nakato, Y. *J. Am. Chem. Soc.* **2003**, *125*, 7443. (b) Sato, S.; Ueda, K.; Kawasaki, Y.; Nakamura, R. *J. Phys. Chem. B* **2002**, *106*, 9054.

(8) (a) Jaeger, C. D.; Bard, A. J. *J. Phys. Chem.* **1979**, *83*, 3146. (b) Howe, R. F.; Grätzel, M. *J. Phys. Chem.* **1987**, *91*, 3906. (c) Micic, O. I.; Zhang, Y.; Cromack, K. R.; Trifunac, A. D.; Thurnauer, M. C. *J. Phys. Chem.* **1993**, *97*, 7277. (d) Grela, M. A.; Coronel, M. E. J.; Colussi, A. J. *J. Phys. Chem.* **1996**, *100*, 16940. (e) Schwarz, P. F.; Turro, N. J.; Bossmann, S. H.; Braun, A. M.; Abdel Wahab, A.-M. A.; Dürr. H. *J. Phys. Chem. B* **1997**, *101*, 7127. (f) Hurum, D. C.; Agrios, A. G.; Gray, K. A.; Rajh, T.; Thurnauer, M. C. *J. Phys. Chem. B* **2003**, *107*, 4545.

(9) (a) Mao, Y.; Schöneich, C.; Asumus, K.-D. *J. Phys. Chem.* **1991**, *95*, 10080. (b) El-Morsi, T. M.; Budakowski, W. R.; Abd-El-Aziz, A. S.; Friesen, K. J. *Environ. Sci. Technol.* **2000**, *34*, 1018.

(10) (a) Nakaoka, Y.; Nosaka, Y. *J. Photochem. Photobiol. A*: *Chem.* **1997**, 110, 299. (b) Nosaka, Y.; Kishimoto, M.; Nishio, J. *J. Phys. Chem. B* **1998**, *102*, 10279. (c) Hirakawa, T.; Nosaka, Y. *Langmuir* **2002**, *18*, 3247.

(11) Nosaka, A. Y.; Fujiwara, T.; Yagi, H.; Akutsu, H.; Nosaka, Y. *Langmuir* **2003**, *19*, 1935.

(12) (a) Draper, R. B.; Fox, M. A. *J. Phys. Chem.* **1990**, *94*, 4628. (b) Draper, R. B.; Fox, M. A. *Langmuir* **1990**, *6*, 1396. (c) Fox, M. A.; Dulay, M. T. *J. Photochem. Photobiol. A*: *Chem.* **1996**, *98*, 91.

(13) (a) Colombo, D. P., Jr.; Bowman, R. M. *J. Phys. Chem.* **1995**, *99*, 11752. (b) Colombo, D. P., Jr.; Bowman, R. M. *J. Phys. Chem.* **1996**, *100*, 18445.

(14) Furube, A.; Asahi, T.; Masuhara, H.; Yamashita, H.; Anpo, M. *Res. Chem. Intermed.* **2001**, *27*, 177.

(15) Tachikawa, T.; Tojo, S.; Fujitsuka, M.; Majima, T. *Chem. Phys. Lett.* **2003**, *382*, 618.

(16) Adamson, A. W.; Gast, A. P. *Physical Chemistry of Surfaces*, 6th ed.; John Wiley & Sons: New York, 1997.

(17) Moser, J.; Punchihewa, S.; Infelta, P. P.; Grätzel, M. *Langmuir* **1991**, *7*, 3012.

(18) (a) Kamat, P. V. *Langmuir*, **1985**, *1*, 608. (b) Kamat, P. V. *J. Phys. Chem.* **1989**, *93*, 859.

(19) Martin, S.; Messelman, J. M.; Park, D. S.; Lewis, N. S.; Hoffmann, M. R. *Environ. Sci. Technol.* **1996**, *30*, 2535.

(20) (a) Meyer, T. J.; Meyer, G. J.; Pfennig, B. W.; Schoonover, J. R.; Timpson, C. J.; Wall, J. F.; Kobusch, C.; Chen, X.; Peck, B. M.; Wall, C. G.; Ou, W.; Erickson, B. W.; Bignozzi, C. A. *Inorg. Chem.* **1994**, *33*, 3952. (b) Weng, Y. X.; Li, L.; Liu, Y.; Wang, L.; Yang, G. Z. *J. Phys. Chem. B* **2003**, *107*, 4356.

(21) Cunningham, J.; Srijaranai, S. *J. Photochem. Photobiol. A*: *Chem.* **1991**, *58*, 361.

(22) Rothenberger, G.; Moser, J.; Grätzel, M.; Serpone, N.; Sharma, D. K. *J. Am. Chem. Soc.* **1985**, *107*, 8054.

(23) Serpone, N.; Lawless, D.; Khairutdinov, R.; Pelizzetti, E. *J. Phys. Chem.* **1995**, *99*, 16655.

(24) Bahnemann, D. W.; Hilgendorff, M.; Memming, R. *J. Phys. Chem. B* **1997**, *101*, 4265.

(25) Bahnemann, D.; Henglein, A.; Lilie, J.; Spanhel, L. *J. Phys. Chem.* **1984**, *88*, 709.

(26) Lawless, D.; Serpone, N.; Meisel, D. *J. Phys. Chem.* **1991**, *95*, 5166.

(27) Rajh, T.; Saponjic, Z. V.; Micic, O. I. *Langmuir* **1992**, *8*, 1265.

(28) (a) Kessler, R. W.; Wilkinson, F. J. *Chem. Soc., Faraday Trans. 1* **1981**, *77*, 309. (b) Wilkinson, F.; Willsher, C. J. *J. Photochem.* **1986**, *33*, 273.

(29) Mohan, H.; Mittal, J. P. *Bull. Chem. Soc. Jpn.* **2001**, *74*, 1649.

(30) Gawandi, V. B.; Mohan, H.; Mittal, J. P. *Res. Chem. Intermed.* **2003**, *29*, 51.

(31) Mohan, H.; Mittal, J. P. *J. Phys. Chem. B* **2002**, *106*, 6574.

(32) Albery, W. J.; Bartlett, P. N.; Wilde, C. P.; Darwent, J. R. *J. Am. Chem. Soc.* **1985**, *107*, 1854.

(33) Thomas, J. K. *Chem. Rev.* **1993**, *93*, 301.

(34) Duonghong D.; Ramsden, J.; Grätzel, M. *J. Am. Chem. Soc.* **1982**, *104*, 2977.

(35) Schwarz, H. A.; Dodson, R. W. *J. Phys. Chem.* **1984**, *88*, 3643.

(36) Cyclic voltammograms were obtained by using a conventional three-electrode system (BAS, CV-50W) in CH_3CN solution at room temperature. A platinum electrode was used as the working electrode and a $Ag/AgNO_3$ electrode was used as the reference electrode.

(37) (a) Rodriguez, R.; Blesa, M. A.; Regazzoni, A. E. *J. Colloid Interface Sci.* **1996**, *177*, 122. (b) Liu, Y.; Dadap, J. I.; Zimdars, D.; Eisenthal, K. B. *J. Phys. Chem. B* **1999**, *103*, 2480. (c) Wang, Y.; Hang, K.; Anderson, N. A.; Lian, T. *J. Phys. Chem. B* **2003**, *107*, 9434.

(38) (a) Colombo, D. P., Jr.; Roussel, K. A.; Saeh, J.; Skinner, D. E.; Cavaleri, J. J.; Bowman, R M. *Chem. Phys. Lett.* **1995**, *232*, 207. (b) Skinner, D. E.; Colombo, D. P., Jr.; Cavaleri, J. J.; Bowman, R. M. *J. Phys. Chem.* **1995**, *99*, 7853.

(39) Linsebigler, A. L.; Lu, G.; Yates, Y. T., Jr. *Chem. Rev.* **1995**, *95*, 735.

(40) (a) Grätzel, M. *Heterogeneous Photochemical Electron Transfer*; CRC Press: Boca Raton, FL, 1989. (b) Hagfeldt, A.; Grätzel, M. *Chem. Rev.* **1995**, *95*, 49. (c) Grätzel, M.; Frank A. J. *J. Phys. Chem.* **1982**, *86*, 2964. (d) Moser, J.; Grätzel, M. *J. Am. Chem. Soc.* **1983**, *105*, 6547.

(41) Marcus, R. A. *J. Phys. Chem.* **1990**, *94*, 1050.

(42) (a) Kuciauskas, D.; Freund, M. S.; Gray, H. B.; Winkler, J. R.; Lewis, N. S. *J. Phys. Chem. B* **2001**, *105*, 392. (b) Ramakrishna, G.; Ghosh, H. N.; Singh, A. K.; Palit, D. K.; Mittal, J. P. *J. Phys. Chem. B* **2001**, *105*, 12786.

(43) (a) Linde, D. R., Ed. *CRC Handbook of Chemistry and Physics*, 73rd ed.; CRC Press: Boca Raton, FL, 1993. (b) *Landolt-Börnstein Numerical Data and Functional Relationships in Science and Technology, New Series*; Hellewege, K. H., Madelung, O., Eds.; Springer-Verlag: Berlin, Germany, 1984; Vol. 17, Subvol. g.

(44) Gould, I. R.; Moser, J. E.; Ege, D.; Farid, S. *J. Am. Chem. Soc.* **1988**, *110*, 1991.

(45) The molecular radius (*a*) was obtained from the density functional theory (DFT) with the GAUSSIAN 98 suite of programs. Molecular volumes of the solutes were calculated by the B3LYP density functional with the standard 6-31G* basis set (B3LYP/6-31G* Volume). The *a* values were determined under the assumption that the solute molecules are spheres. Frisch, M. J.; Trucks, G. W.; Schlegel, H. B.; Scuseria, G. E.; Robb, M. A.; Cheeseman, J. R.; Zakrzewski, V. G.; Montgomery, J. A., Jr.; Stratmann, R. E.; Burant, J. C.; Dapprich, S.; Millam, J. M.; Daniels, A. D.; Kudin, K. N.; Strain, M. C.; Farkas, O.; Tomasi, J.; Barone, V.; Cossi, M.; Cammi, R.; Mennucci, B.; Pomelli, C.; Adamo, C.; Clifford, S.; Ochterski, J.; Petersson, G. A.; Ayala, P. Y.; Cui, Q.; Morokuma, K.; Malick, D. K.; Rabuck, A. D.; Raghavachari, K.; Foresman, J. B.; Cioslowski, J.; Ortiz, J. V.; Baboul, A. G.; Stefanov, B. B.; Liu, G.; Liashenko, A.; Piskorz, P.; Komaromi, I.; Gomperts, R.; Martin, R. L.; Fox, D. J.; Keith, T.; Al-Laham, M. A.; Peng, C. Y.; Nanayakkara, A.; Gonzalez, C.; Challacombe, M.; Gill, P. M. W.; Johnson, B.; Chen, W.; Wong, M. W.; Andres, J. L.; Gonzalez, C.; Head-Gordon, M.; Replogle, E. S.; Pople, J. A. *Gaussian 98*; Gaussian, Inc.: Pittsburgh, PA, 1998.

(46) Enright, B.; Fitzmaurice, D. *J. Phys. Chem.* **1996**, *100*, 1027.

(47) Palik, E. D. *Handbook of Optical Constants of Solids*; Academic Press: New York, 1984.

(48) Weng, Y.-X.; Wang, Y.-Q.; Asbury, J. B.; Ghosh, H. N.; Lian, T. *J. Phys. Chem. B* **2000**, *104*, 93.

(49) Clifford, J. N.; Yahioglu, G.; Milgrom, L. R.; Durrant, J. R. *Chem. Commun.* **2002**, 1260.

(50) Yokoi, H.; Hatta, A.; Ishiguro, K.; Sawaki, Y. *J. Am. Chem. Soc.* **1998**, *120*, 12728.